Synthesis of 4-Chloro-1,3-Diazobenzene Bent-Cores Liquid Crystals and Characterizations of Their Mesogenic Behaviors and Photoisomerization Phenomena

Jinying Lu[a], Zelong Zhang[b*], Daoren Yan[a], Zhiyong Zhang[a]*, Jintao Guan[a], and Junfei Qiao[a]

[a]Department of Chemistry and Environmental Engineering, Wuhan Polytechnic University, Wuhan, China; [b]Department of Geology and Geophysics, Louisiana State University, Baton Rouge, LA, USA

Corresponding authors*

Dr. Zelong Zhang zelongz@lsu.edu

Mr. Zhiyong Zhang zzy6211@126.com

Abstract

Azobenzene-based bent-core liquid crystals demonstrate a variety of mesomorphic behaviors and photochromic properties which are desirable for optical switching. Nowadays azobenzene-based bent-core liquid crystal (ABLC) compounds usually exhibit at least one of the following traits which are unfavorable for practical applications: (1) narrow temperature windows of nematic phases, (2) high phase transition temperature, and (3) long period of light stimulation to reach photostationary states. In this study, a series of ABLC compounds **4a–4g** were synthesized by adding azo functional groups and chlorine substituent to the central bent-cores to form 4-chloro-1,3-dizaophenylene bent-cores. These ABLC compounds were characterized by i. fourier-transform infrared spectroscopy (FTIR), ^{1}H and ^{13}C nuclear magnetic resonance (NMR), and mass spectrometry (MS) for their structures, ii. differential scanning calorimetry (DSC) and polarized optical microscopy (POM) for their mesogenic properties, and iii. ultraviolet–visible spectroscopy (UV-Vis) and POM for their photosensitivity. The experimental results show that all compounds exhibited broad temperature windows of mesogenic phases. In particular, compound **4c** showed a broad temperature window of 63.8 °C for nematic phase. Molecular simulations indicate that the molecular dipole moments of compounds **4a–4g** are closely associated with the temperatures of Sm – N phase transition and temperature ranges of nematic phases. In addition, simulation results reveal that the terminal alkyl chains exhibit a diphasic effect on the molecular polarity: extending the terminal chain can initially reduce and then increase the molecular dipole moments due to the severe structural disorder of overly extended terminal chain. These findings indicate that the intermolecular forces play a vital role in shaping the mesogenic behavior of ABLCs. Comprehensive characterizations of photochromatic properties show that **4c** was highly photosensitive and displayed rapid photoisomerization processes. At room temperature, compound

4c dissolved in ethyl acetate solution can reach photostationary state in 10 seconds. At 95 °C, compound **4c** in nematic phase became isotropic liquid under UV-irradiation in 3 seconds due to the forward *trans – cis* photoisomerization and can be restored to be nematic under natural visible light in 5 seconds because of the backward *cis – trans* photoisomerization. This study linking the mechanistic details with mesogenic properties provides valuable insights to improve future design of azobenzene bent-core liquid crystals for practical applications especially in photonic applications.

Keywords:

bent-core liquid crystal; 4-chloro-1,3-diazobenzene; synthesis; nematic phase; photoisomerization; molecular mechanics simulation.

1. Introduction

Signal switch is vital to the data transmission in communication and information technology. Photonic technology such as optical fiber has tremendous bandwidth compared to electrical technology because of the significantly weaker interactions between photons than that of electrons.[1] However, current design of optical switch still requires electrical control due to the limitation of materials, which hinders the deployment of photonic technology to a larger scale. Therefore, discovering new materials which can be tunable by photon is critical to the future design of optical switch.[1–3]

Photosensitive liquid crystals, especially azobenzene-based bent-core liquid crystals (ABLCs), are promising materials for optical switching.[4–7] ABLC compounds can be highly photochromic and mesogenic due to the reversible *trans-cis* photoisomerization of azo group (–N=N–) induced by proper irradiation of ultraviolet or visible light.[8,9] These characteristics also give rise to a myriad of potential applications of ABLC in areas such as elastomer, holographic imaging, optical data storage, and nanomachines.[10–14]

To date, the majority of ABLC compounds implemented at least one ester as the direct linkage of the central bent-core and or deployed azo groups in the distant side arms,[8,15–20] which usually exhibited high temperatures of phase transition, far above room temperature 25 °C, and narrow temperature ranges of nematic phases. To lower the phase transition temperature and broaden the temperature range of nematic phases, recent studies emphasized on structural alterations such as introducing different lateral substitutions on the bending core, [15,16,21] adjusting the number of aromatic units,[17,22–24] modifying the type, number, and position of linkage groups,[17,25–28] and changing the type and length of the terminal chains.[17,18,28–30] Yet, the mesogenic phase behaviors of current ABLCs are still unfavorable for practical applications.

We hypothesized that the linking groups adjacent to the central bent-core play a vital role in determining the mesogenic properties of ABLCs. The ester groups commonly used on the central bent-cores as the linking units can induce strong electrostatic forces that contribute to the intermolecular interactions of ABLCs, leading to high phase transition temperatures and narrow nematic phases. Previous studies suggest that the location of azo linkage does not exert significant influence on the mesogenic behavior; if azo bond is close to central ring, it can even inhibit the formation of mesogenic phases.[17,25] However, their conclusions were based on compounds with a single azo linkage. This study proposed an alternative approach to improve the design of ABLCs by using two azo bonds instead of esters as the central linkages connecting the central bent-core, which intends to weaken the intermolecular interactions and therefore to enhance the overall performance of ABLCs. ABLC compounds synthesized in this study were derived from 4-chloro-1,3-diazobenzene. They all have two azo linkages and one chlorine substituent in the 1,3-position and 4-position, respectively, at the central aromatic ring and terminal alkyl chains of different length ranging from 5 to 12 carbon atoms (**4a–4g** in Figure 1 and 5).

2. Materials and methods

2.1 Materials

Anhydrous aluminum trichloride (chemically pure), N, N'-dicyclohexylcarbodiimide (DCC), and 4-dimethylaminopyridine (DMAP) were obtained from Tianjin Fuchen Chemical Reagent (China), Nanjing Chemical Reagent (China), and Xiya Reagent (China), respectively. All chemicals used in this study are of analytical grade, unless otherwise stated. 4-n-hexylbenzoic acid, 4-n-heptylbenzoic acid, 4-n-octylbenzoic acid, 4-n-decylbenzoic acid, and 4-n-decylbenzoic acid were synthesized in our laboratory. Reaction products were purified by silica gel column chromatography and recrystallized three times from ethanol – dichloromethane 1:1 mixture.

2.2 Characterization

Reactions required low temperature were conducted in Zhengzhou Greatwall DHJF-8002 low temperature constant temperature stirring reaction bath. Infrared spectroscopy was performed by a Thermo Nicolet Avatar 330 FTIR. ^{1}H NMR spectra were obtained from a Varian INOVA 400 spectrometer (400 MHz) using tetramethylsilane (TMS) as the reference standard. Differential scanning calorimetry (DSC) experiments were conducted on a TA Instruments DSC Q-20 with a scanning rate of 5 °C/ min and natural cooling. Phase transition and optical textures of liquid crystal compounds were characterized by a polarizing optical microscope (POM) XPN-100E from Shanghai Changfang Optical Instrument.

UV-Visible absorption spectroscopy was collected by a UV-8000S spectrophotometer from Shanghai Metash Instrument. UV-Vis experiments were conducted using a wavelength range from 200 nm to 550 nm and a scan rate of 1 nm/s. UV-Vis spectral data were used i. to measure the isomer fraction by dissolving sample in dilute solution of ethyl acetate (2.5×10^{-5} mol/L) at room temperature and ii. to characterize the UV-induced photoisomerization of mesogenic phases at 95 – 100 °C. The data collection of UV-Vis spectroscopy was started when the absorbance value of the two consecutive measurements were identical.

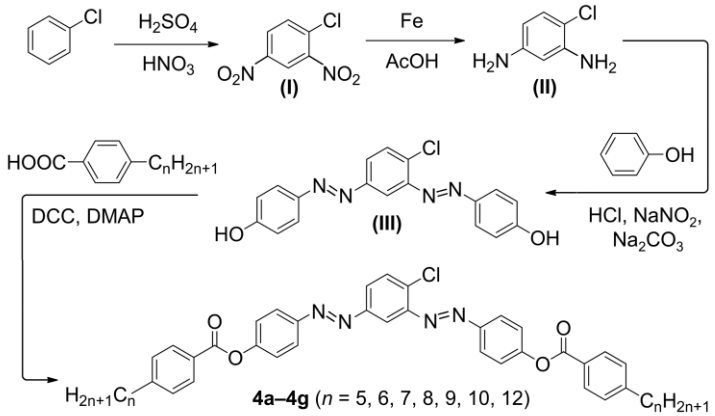

Figure 1. Synthesis of 4-chloro-1,3-diazobenzene bent-core liquid crystals **4a–4g**.
"*n*" denotes the number of carbon atoms in the terminal alkyl chains.

2.3 Synthesis

Compounds **4a–4g** were synthesized according to Figure 1, of which the steps were described below.

2.3.1 Synthesis of 4-chloro-1,3-dinitrobenzene **(I)**[31]

Chlorobenzene (40 ml) was added in a 500 ml three-neck flask with magnetic stir bar. The temperature was maintained at 95 °C. Concentrated nitric acid (117.6 ml) and concentrated sulfuric acid (123.6 ml) were added in the flask. The solution mixture was stirred for 5 hours, in which the reaction was monitored by thin layer chromatography (TLC). The reaction product was washed with hot water to reach pH neutral, vacuum-filtered, and air-dried. This step produced yellow crystals.

Yield: 55.07 g, 85.2%, melting point (m.p.) 48 °C. FTIR (KBr, ν_{max}, cm^{-1}): 3082.32 (Ar–H), 1618.15, 1528.35 (Ar), 1474.40, 1352.32, 1306.78, 1202.84, 1102.45.

2.3.2. Synthesis of 4-chlorom-1,3-diaminobenzene **(II)**[32]

pure iron powder (28 g, 0.5 mol), glacial acetic acid (45 g), and 100 mL deionized water were added in a 250 mL three-necked flask. Once the solution was heated to 70 ~ 80 °C, compound (**I**) (20.2 g, 0.1 mol) was added. The reaction was carried out for 4h, which was monitored by TLC to ensure the completion. The product mixture was filtered and washed with hot water two times to remove the nonpolar impurities. The pH of the filtrate was adjusted to pH 10.0 with saturated Na_2CO_3 solution. The organic phase was extracted with 30 mL ethyl acetate repeated for three times and then was dried with anhydrous K_2CO_3, yielding a crude black product. The product was purified by silica gel column chromatography. This step produced a needle-shaped brown solid of compound (**II**).

Yield: 10.5 g, 74.2%, m.p. 86-88 °C. FTIR (KBr, ν_{max}, cm^{-1}): 3343.37, 3405.11, 3315.06 (N–H), 3211.17 (Ar–H), 1615.53, 1577.97, 1496.67, 1451.98 (Ar), 1333.37, 1274.30, 1208.48, 1147.56, 1106.67, 1044.15, 845.96.

2.3.3 Synthesis of 4-chloro-1,3-bis (4-hydroxyphenyl)azobenzene **(III)**[33]

Chilled concentrated hydrochloric acid (40 mL, 0.5mol) was added in a three-necked flask. The temperature was maintained below –25 °C. A solution prepared from sodium nitrite (12.5 g, 0.18 mol) and 19 mL deionized water was added dropwise while stirring slowly. Then, a solution prepared from compound (**II)** (7.15g, 0.05mol) and concentrated hydrochloric acid (25mL) was added in multiple steps while gradually increasing the stirring speed. The reaction was lasted for 0.5 hour, generating a yellow transparent liquid. Urea pellets (4.8 g, 0.08mol) were added into the liquid dropwise while stirring to yield a diazonium salt.

The diazonium salt was added slowly to a three-necked flask containing a solution of phenol (11.3g, 0.12mol), sodium carbonate (31.8g, 0.3mol) and water (200ml). The mixture in the flask was stirred for 3h in a cold-water bath, of which the reaction was monitored by the TLC. Once the reaction was completed, the mixture was filtered. The resultant filter cake was recrystallized from ethanol. 10.96g of yellow crystals of compound (**III**) was obtained. Yield: 62.3%. m.p. 164 ~ 166 °C. FTIR (KBr, ν_{max}, cm^{-1}): 3333.1 (–OH), 1702.11, 1583.27, 1502.13, 1473.53 (Ar), 1256.44, 1223.10, 1192.22, 1069.13, 1028.42, 853.33; ^{1}H NMR (400 MHz, $CDCl_3$, δ, ppm): 8.31 (s, 1H), 7.95 ~ 7.97 (d, J = 8 Hz, 1H), 7.67 ~ 7.77 (m, 5H), 7.18 ~ 7.21 (t, J = 6 Hz, 4H), 5.08 (s, 2H); ^{13}C NMR (100 MHz, $CDCl_3$): 161.118, 152.732, 149.855, 130.145, 129.282, 124.259, 120.387, 118.365, 115.927. MS m/z (%): 353.65 (65.5, M+1), 231.67 (19.5), 111.67 (13.1).

2.3.4 Synthesis of ABLC compounds **4a–4g**[34]

Compound (**II**) (1.66 g, 5mmol), 4-alkylbenzoic acid (10mmol), DCC (12 mmol), DMAP (1.2 mmol) and CH_2Cl_2 (50mL) were added in a 100 mL three-necked flask. The mixture was stirred at room temperature for 24 hours, in which this reaction was monitored by TLC. Upon the completion of the reaction, the mixture was filtered and washed with CH_2Cl_2. The solute was extracted by evaporating the solvent under reduced pressure and then purified by silica gel column chromatography.

4-Chloro-1,3-bis(4-((4-pentylphenyl)acyloxy)-1-(E)-azophenyl)benzene **4a**: 2.52g yellow solid flakes, yield: 75.8%. m.p: 103 ~ 104 °C. FTIR (KBr, ν_{max}, cm^{-1}): 2930.13, 2851.70 (-CH_2-), 1680.54, 1643.95, 1613.23, 1546.77, 1507.93, 1447.28 (Ar), 1354.67, 1337.28, 1276.20, 1236.88, 1128.86, 1078.87. ^{1}H NMR (400 MHz, $CDCl_3$): δ (ppm): 8.46 (s, ^{1}H), 8.13 ~ 8.15 (d, J = 6 Hz, 4H), 8.05 ~ 8.07 (d, J = 9 Hz, 4H), 7.66 ~ 7.68 (t, J = 7.8 Hz, 1H), 7.39 ~ 7.41 (d, J = 6.5 Hz, 4H), 7.31 ~ 7.33 (d, J = 6.5 Hz, 4H), 2.68 ~ 2.70 (t, J = 4 Hz, 4H), 1.54 ~ 1.64 (m, 4H), 1.30 ~ 1.36 (m, 8H), 0.875 ~ 0.89 (t, J = 6 Hz, 6H). ^{13}C NMR (100 MHz, $CDCl_3$) δ (ppm): 164.929, 153.388, 153.342,150.142, 149.719, 130.365, 129.702, 128.773, 126.640, 125.442, 124.367, 122.531, 116.501, 36.149, 31.935, 31.172, 22.726, 14.171. MS m/z (%): 701.64 (72.5, M+1), 497.62 (13.6), 351.57 (22.3).

4-Chloro-1,3-bis(4-((4-hexylphenyl)acyloxy)-1-(E)-azophenyl)benzene **4b**: 2.45g yellow solid flakes, yield: 7.23g, m.p. 92 ~ 93 °C. FTIR (KBr, ν_{max}, cm^{-1}): 2952.11 (–CH2), 2441.50, 1675.36, 1623.45, 1623.13, 1556.78, 1517.83, 1457.24 (Ar), 1356.69, 1327.18, 1256.10, 1246.82, 1158.86, 998.87. ^{1}H NMR (400 MHz, $CDCl_3$) δ (ppm): 8.55 (s, 1H), 8.21 ~ 8.23 (d, J = 6.5 Hz, 4H), 8.125 ~ 8.15 (d, J = 9 Hz, 4H), 7.84 ~ 7.86 (t, J = 6.5 Hz, 1H), 7.41 ~ 7.43 (d, J = 7.8 Hz, 4H), 7.32 ~ 7.34 (d, J = 6.5 Hz, 4H), 2.70 ~ 2.72 (t, J = 5Hz, 4H), 1.62 ~ 1.65 (m, 4H), 1.31 ~ 1.38

(m, 12H), 0.90 ~ 0.92 (t, J = 6Hz, 6H); ^{13}C NMR (100 MHz, $CDCl_3$) δ (ppm): 164.929, 153.388, 153.342, 150.142, 149.719, 130.365, 129.702, 128.773, 126.640, 125.442, 124.367, 122.531, 116.501, 36.149, 31.935, 31.172, 29.325, 22.726, 14.171. MS m/z (%): 729.53 (55.25, M+1), 587.62 (15.4), 351.54 (20.3).

4-Chloro-1,3-bis(4-((4-heptylphenyl)acyloxy)-1-(E)-azophenyl)benzene **4c**: 2.48g yellow needle crystal, yield: 71.5%, m.p. 84 ~ 85.5 °C. FTIR (KBr, ν_{max}, cm^{-1}): 2918.17, 2849.16 (–CH2), 1169.63, 1645.76, 1613.79, 1542.68, 1507.81, 1450.59 (Ar), 1355.50, 1339.12, 1296.69, 1233.43, 1125.32, 841.01. ^{1}H NMR (400 MHz, $CDCl_3$) δ (ppm): 8.32 (s, 1H), 8.09 ~ 8.11 (d, J = 6.5 Hz, 4H), 7.99 ~ 8.01 (d, J = 8 Hz, 4H), 7.53 ~ 7.55 (t, J = 6.5 Hz, 1H), 7.18 ~ 7.20 (d, J = 8 Hz, 4H), 7.07 ~ 7.09 (d, J = 6.0 Hz, 4H), 2.60 ~ 2.63 (t, J = 6 Hz, 4H), 1.63 ~ 1.66 (m, 4H), 1.31 ~ 1.36 (m, 16H), 0.89 ~ 0.92 (t, J = 6 Hz, 6H). ^{13}C NMR (100 MHz, $CDCl_3$) δ (ppm): 164.819, 152.378, 152.352, 150.212,149.701, 130.321, 129.732, 128.715, 126.590, 125.356, 124.289, 122.425, 116.423, 36.222, 31.852, 31.225, 30.285, 29.285, 22.589, 14.152. MS m/z (%): 757.59 (71.10，M+1), 587.70 (16.5), 295.58 (28.1).

4-Chloro-1,3-bis(4-((4-n-octylphenyl)acyloxy)-1-(E)-azophenyl)benzene **4d**: 2.66g yellow needle crystal, yield: 75.2%, m.p. 76 ~ 77 °C. FTIR (KBr, ν_{max}, cm^{-1}): 2928.13 (–CH2), 2441.70, 1166.54, 1632.95, 1615.23, 1532.77, 1511.93, 1454.28 (Ar), 1348.67, 1342.28, 1286.20, 1228.88, 1138.86, 886.25. ^{1}H NMR (400 MHz, $CDCl_3$) δ (ppm): 8.43 (s, 1H), 8.17 ~ 8.19 (d, J = 6.5 Hz, 4H), 8.03 ~ 8.05 (d, J = 8.8 Hz, 4H), 7.66 ~ 7.68 (t, J = 6.0 Hz, 1H), 7.36 ~ 7.38 (d, J = 5 Hz, 4H), 7.29 ~ 7.31 (d, J = 6 Hz, 4H), 2.68 ~ 2.71 (t, J = 6Hz, 4H), 1.65 ~ 1.68 (m, 4H), 1.32 ~ 1.37 (m, 20H), 0.89 ~ 0.92 (t, J = 6 Hz, 6H). ^{13}C NMR (100MHz, $CDCl_3$) δ (ppm): 164.759, 153.258, 153.452, 150.322, 149.899, 130.425, 129.882, 128.123, 126.540, 125.112, 124.337, 122.441, 116.551, 36.229, 31.985, 31.122, 30.255, 29.852, 29.285, 22.526, 14.151. MS m/z (%):

785.72 (50.45, M+1), 351.60 (11.7), 295.68 (27.4).

4-Chloro-1,3-bis(4-((4-n-nonylphenyl)acyloxy)-1-(E)-azophenyl)benzene **4e**: 2.55 g yellow flake solid, yield: 70.8%, m.p. 73 ~ 74 °C. FTIR (KBr, ν_{max}, cm^{-1}): 2920.13, 2861.70 (–CH2), 1166.54, 1164.97, 1622.32, 1536.67, 1517.83, 1457.32 (Ar), 1344.57, 1347.18, 1266.10, 1246.78, 1340.46, 959.21. ^{1}H NMR (400 MHz, $CDCl_3$) δ (ppm): 8.36 (s, 1H), 8.24 ~ 8.26 (d, J = 6.5 Hz, 4H), 8.08 ~ 8.10 (d, J = 8 Hz, 4H), 7.58 ~ 7.60 (t, J = 4 Hz, 1H), 7.38 ~ 7.40 (d, J = 6.5 Hz, 4H) 7.31 ~ 7.33 (d, J = 6.5 Hz, 4H), 2.77 ~ 2.80 (t, J = 6 Hz, 4H), 1.70 ~ 1.74 (m, 4H), 1.35 ~ 1.41 (m, 24H), 0.88 ~ 0.91 (t, J = 6 Hz, 6H). ^{13}C NMR (100 MHz, $CDCl_3$) δ (ppm): 164.829, 153.348, 153.522, 150.322, 149.889, 130.325, 129.652, 128.553, 126.650, 125.322, 124.427, 122.551, 116.441, 36.259, 31.335, 31.152, 30.255, 30.145, 30.025, 29.255, 22.746, 14.131. MS m/z (%): 813.65 (55.5, M+1), 351.71 (17.6). 203.31 (15.5).

4-Chloro-1,3-bis(4-((4-n-decylphenyl)acyloxy)-1-(E)-azophenyl)benzene **4f**: 2.57g yellow needle crystal, yield: 69.8%. m.p: 65 ~ 66 °C. FTIR (KBr, ν_{max}, cm^{-1}): 2920.01, 2850.68 (–CH2), 1728.64, 1608.83, 15993.34, 1496.65, 1466.78, 1416.72 (Ar), 1266.35, 1209.43, 1174.94, 1145.96, 1066.17, 1017.92. ^{1}H NMR (400 MHz, $CDCl_3$) δ (ppm): 8.46 (s, 1H), 8.14 ~ 8.16 (d, J = 6.4 Hz, 4H), 8.06 ~ 8.08 (d, J = 8 Hz, 4H), 7.68 ~ 7.69 (t, J = 4 Hz, 1H), 7.38 ~ 7.40 (d, J = 8 Hz, 4H), 7.33 ~ 7.34 (d, J = 6 Hz, 4H), 2.70 ~ 2.73 (t, J = 6 Hz, 4H), 1.65 ~ 1.68 (m, 4H), 1.31 ~ 1.35 (m, 28H), 0.90 ~ 0.93 (t, J = 6 Hz, 6H). ^{13}C NMR (100 MHz, CDCl3) δ (ppm): 164.939, 153.378, 153.332, 150.132, 149.729, 130.315, 129.722, 128.783, 126.650, 125.421, 124.363, 122.542, 116.456, 36.222, 31.895, 31.212, 30.225, 30.112, 30.005, 29.855, 29.255, 22.756, 14.161. MS m/z (%): 841.46 (75.10, M+1), 351.66 (22.7), 231.05 (16.8).

4-Chloro-1,3-bis(4-((4-n-dodecylphenyl)acyloxy)-1-(E)-azophenyl)benzene **4g**: 2.72g yellow crystal, yield: 71.2%, m.p. 70.5 ~ 71.5 °C. FTIR (KBr, ν_{max}, cm^{-1}): 2912.13, 2821.70 (–

222 CH_2), 1750.54, 1523.95, 1655.23, 1506.77, 1544.93, 1420.28 (Ar), 1254.67, 1237.28, 1176.20,
223 1136.88, 1028.86, 1001.87. ^{1}H NMR (400 MHz, $CDCl_3$) δ (ppm): 8.46 (s, 1H), 8.13 ~ 8.15 (d, J =
224 6 Hz, 4H), 8.05 ~ 8.08 (d, J = 8.5 Hz, 4H), 7.67 ~ 7.69 (t, J = 4.5 Hz, 1H), 7.39 ~ 7.41 (d, J = 6.5
225 Hz, 4H), 7.32 ~ 7.34 (d, J = 6 Hz, 4H), 2.69 ~ 2.72 (t, J = 6Hz, 4H), 1.64 ~ 1.67 (m, 4H), 1.30 ~
226 1.40 (m, 36H), 0.89 ~ 0.91 (t, J = 6 Hz, 6H). ^{13}C NMR (100 MHz, $CDCl_3$) δ (ppm): 164.929,
227 153.388, 153.342, 150.142, 149.719, 130.365, 129.702, 128.773, 126.640, 125.442, 124.367,
228 122.531, 116.501, 36.149, 31.935, 31.172, 30.855, 30.255, 30.155, 30.022, 29.875, 29.657, 29,285,
229 22.726, 14.171. MS m/z (%): 897.54 (60.5, M+1), 245.31 (23.8), 351.62 (28.3).

230 *2.3.4 Molecular Simulation*

231 To validate the hypothesis based on experimental data, molecular simulations were
232 performed to study the molecular geometry and molecular dipole moments at the ground states.
233 The compounds of interest in this study contain 92 ~ 134 atoms and 6 ~ 10 rotatable bonds.
234 Quantum mechanics methods are not preferable for this purpose due to the high computation cost.
235 Therefore, molecular mechanics simulations were applied given its reasonable computation cost
236 and capability to provide atomistic details.

237 Molecular simulations were performed on Avogadro 1.2.0 software.[35,36] General Amber
238 force field (GAFF) was used due to its specific parameterization for organic molecules,[37,38] which
239 has successfully described mesogenic behaviors.[39,40] Geometry optimization was conducted using
240 steepest descent algorithm with convergence energy 10^{-7} kcal/mol. Input structural parameters of
241 azobenzene moiety were adopted from previous density functional theory calculation and X-ray
242 diffraction data.[41,42] To find the conformers of the lowest energy, random rotor search and Genetic
243 algorithm search were carried out.

3. Results and discussion

In this study, each ABLC compound comprises a 4-Cl-1,3-m-phenylene rings as the central bent cores, two azo bonds as the linkages of the central core, two ester groups as lateral arm bridges, and linear alkyl groups as the terminal chains. In total, seven ABLC compounds **4a–4g** with varying length of terminal alky chains were synthesized. All these compounds were characterized by FTIR, ^{1}H NMR, ^{13}C NMR, and mass spectrometry. Their mesogenic properties were examined by DSC and POM. Photoisomerization phenomena were characterized by UV-Vis spectroscopy. The experimental results show that (1) the structure of compounds **4a–4g** are consistent with our design and (2) **4a–4g** all exhibited low melting points and wide temperature windows of nematic phase. The effects of terminal alkyl groups and azo groups on the phase transitions are also discussed.

3.1 Phases transition temperatures and enthalpies of compounds 4a–4g

The phases, transition temperatures, and transition enthalpies of compounds **4a–4g** are listed in Figure 2 – 3 and Table 1. DSC analysis in Figure 2 shows that while increasing temperature

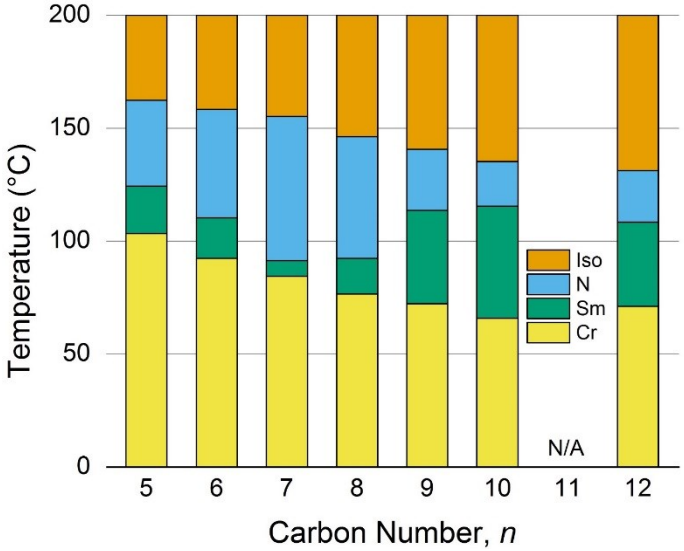

Figure 2. Phase transition temperatures of compounds **4a–4g**. Yellow, pink, cyan, and grey blocks represent crystalline (Cr) solid, smectic (Sm) phase, nematic (N) phase, and isotropic (Iso) phase, respectively.

Table 1. Phase transition temperatures of compound **4a–4g**. "*n*" denotes the carbon number in the terminal alkyl chain; "Cr – Sm" phase transition from crystalline phase; "Sm" the smectic phase; "N" the nematic phase; "Iso" the isotropic liquid; "T" the phase transition temperature in °C; "ΔH" the reaction enthalpy in kJ/mol; "ΔT_{LC}" the temperature window of liquid crystal phase in °C; "ΔT_N" the temperature window of nematic phase in °C.

Compound	*n*	**Cr – Sm**		**Sm – N**		**N – Iso**		ΔT_{LC}	ΔT_N
		T	ΔH	T	ΔH	T	ΔH		
4a	5	103.37	30.3	124.36	8.05	162.36	4.7	58.99	38.00
4b	6	92.38	34.1	110.36	8.9	158.36	2.6	65.98	48.00
4c	7	84.52	33.7	91.36	7.4	155.2	2.95	70.68	63.84
4d	8	76.56	37.9	92.35	7.6	146.23	3.8	69.67	53.88
4e	9	72.35	41.3	113.65	8.9	140.62	2.8	68.27	26.97
4f	10	65.92	38.8	115.46	12.7	135.26	3.2	69.34	19.80
4g	12	71.2	52.3	108.36	19	131.26	4.5	60.06	22.90

all compounds **4a–4g** displayed the following phases: crystalline solid (Cr), smectic (Sm), nematic (N), and isotropic liquid (Iso). The temperatures of phase transition are ranging from 65.92 °C to 103.37 °C for Cr – Sm, 91.36 °C to 124.36 °C for Sm – N, and 131.26 °C to 162.36 °C for N – Iso. Figure 3 shows that the enthalpies for Cr – Sm, Sm – N, and N – Iso transitions are ranging from 30.3 kJ/mol to 52.3 kJ/mol, 7.4 kJ/mol to 19 kJ/mol, and 2.6 kJ/mol to 4.7 kJ/mol, respectively.

The terminal chain length demonstrates a pronounced and systematic effect on the phase transition of **4a–4g**. Overall, as the carbon number (n) in the terminal alkyl chains increases, the phase transition temperatures decrease except for the Sm – N transition and transition enthalpies increases except for the N – Iso transition. However, the temperatures of Sm – N transition were initially decreasing and then increasing as the carbon number increases. The impact from carbon number to the N – Iso transition enthalpies was insubstantial.

Figure 2 shows that generally the phase transition temperatures decrease over the increment of carbon number (*n*) in the terminal alkyl chains. Notably, the phase transition temperatures of N – Iso exhibited a linear relationship with respect to the carbon number, giving a linear fitting with a R^2 (the coefficient of determination) of 0.96. A similar trend was also found for the phase transition of Cr – Sm, which gives a R^2 of 0.96 if treating the data of compound **4g** as an outlier. However, the linear relationship between the Sm – N transition temperatures and the carbon number is insubstantial with a R^2 of 0.01, which indicates the phase behaviors in Sm – N transition are inconsistent with those in the other phase transitions. The only structural difference between compounds **4a–4g** is the length of terminal alkyl chain. Therefore, the inconsistent changes in phase behavior during Sm – N transition could be attributed to the structural difference associated with the terminal chains of compound **4a–4g** during this phase transition.

Additionally, as shown in Table 1, the liquid crystal phases transition temperature of compound **4a–4g** generally exhibited wide temperature windows of both mesogenic phases ranging from 58.99 °C to 70.68 °C and nematic phases ranging from 19.89 °C to 63.84 °C. In particular, the widest temperature window of mesogenic phase (70.68 °C) and nematic phase

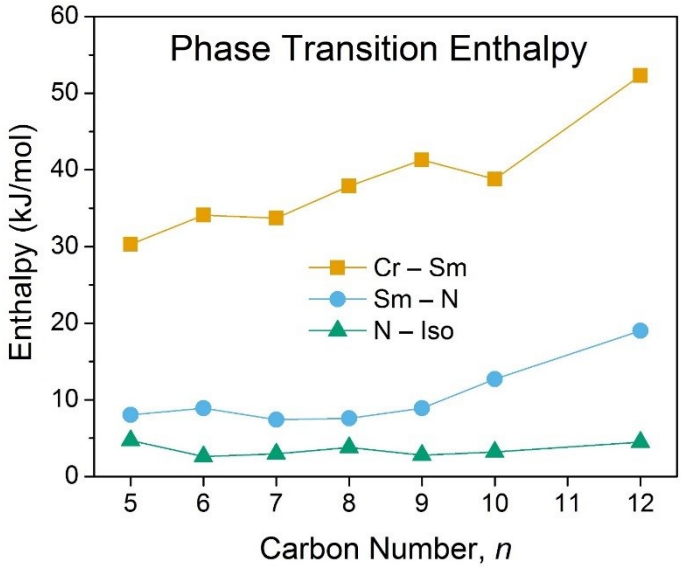

Figure 3. Enthalpies for the phase transitions of compounds **4a–4g**.

(63.84 °C) were both exhibited by compound **4c**, which has a moderate length of terminal chains (n = 7). The narrowest temperature window for nematic phase (19.8 °C) was exhibited by compound **4f**, which also has the lowest melting point 65.9 °C.

A previous study shows that the liquid crystal compounds can exhibit a systematic odd-even periodic pattern on phase transition properties according to the carbon number in the terminal alkyl chains.[43–47] Through closer examinations, we noticed that the changes in melting points, clearing points, and enthalpies exhibit similar odd-even pattern as shown in Figure 2 and 3.

3.2 Biphasic effect of terminal chain length

At the molecular scale, phase transition is the rearrangement of molecules. Phase transitions of nematic liquid crystals are intrinsically associated with the intermolecular interactions especially the long-range non-bonded electrostatic interactions.[48–52] Therefore, it is necessary to examine the molecular properties such as molecular polarity that determine the intermolecular electrostatic interactions.[50,53,54] The degree of molecular polarity can be assessed

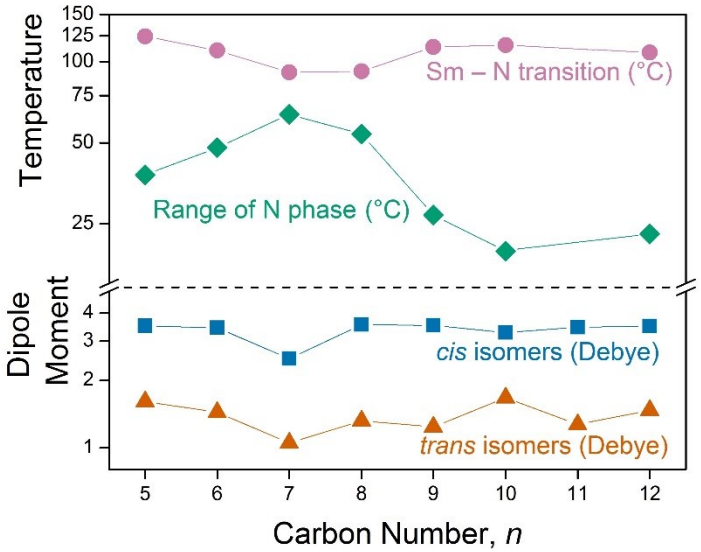

Figure 4. Comparison between the Sm – N phase transition temperatures, temperature ranges of nematic phases, and dipole moments of trans and cis isomers of **4a–4g** with respect to the carbon numbers (n) in the terminal alkyl chains.

by measuring molecular dipole moment.[50,53,54] The molecular dipole moments of **4a–4g** were computed based on their isomer structures in the ground states.

As listed in Table 2, the dipole moments of isomers of **4a–4g** are ranging from 1.05 to 1.67 Debye and 2.50 to 3.55 Debye for *trans* and *cis* isomers, respectively. Figure 4 plots the dipole moments against the carbon number (*n*) of the terminal chains, which shows similar trends for both isomers: increment in the carbon number initially reduces the molecular dipole moments in the *n* range of 5 to 7 and then increases the dipole moments in the *n* range of 8 to 12. The smallest dipole moments were created by compound **4c** isomers with $n = 7$. In addition, Figure 4 also compares Sm – N transition temperatures and temperature ranges of nematic phase of **4a–4g** compounds with their corresponding dipole moments. This comparison shows that the impact from terminal chain length to the dipole moments remarkably resembles that of the phase transition temperatures of Sm – N, whereas the effect of terminal chains on the temperature ranges of nematic phase appears to be the opposite. Notably, among compound **4a – 4g**, **4c** exhibits the smallest

Table 2. Molecular dipole moments of compound **4a–4g** calculated by Avogadro using GAFF force field and steepest descent algorithm. "*n*" denotes the number of carbon atoms in each terminal alkyl chain.

Compound	*n*	Dipole moment (Debye)	
		trans isomer	*cis* isomer
4a	5	1.61	3.50
4b	6	1.44	3.44
4c	7	1.05	2.50
4d	8	1.32	3.55
4e	9	1.24	3.52
4f	10	1.67	3.28
N/A	11	1.27	3.45
4g	12	1.47	3.53

311 dipole moment, the lowest temperature of Sm – N phase transition, and the widest range of nematic
312 phase. These patterns show that the molecular dipole moments can indicate the degree of
313 intermolecular interactions in nematic phase, which implies that the nematic phase is the domain
314 of the long-range electrostatic interactions. In addition, an apparent odd-even periodic pattern of
315 dipole moments with respect to the carbon number was observed, which is consistent with our
316 measurements of the phase transition properties.

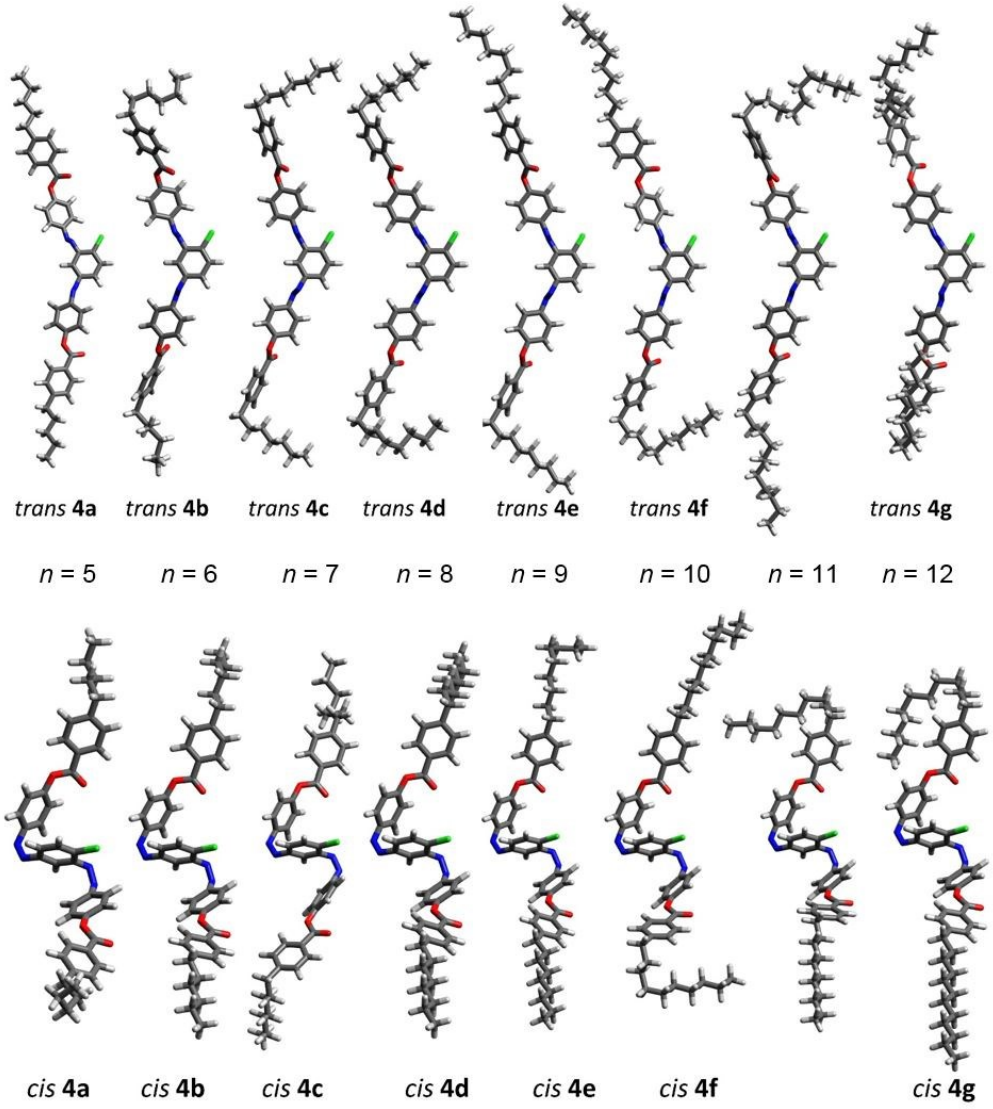

Figure 5. Molecular structures of *trans* and *cis* isomers of **4a**–**4g** in the ground state computed by molecular mechanics simulations.

Figure 5 lists the molecular geometries of both *trans* and *cis* isomers of compounds **4a–4g** at the ground state, which were predicated by molecular mechanics simulations. The result shows that varying the length of terminal alkyl chains has no apparent impact on the structure of central units with five aromatic rings but causes substantial changes to the structures of terminal alkyl chains. As the carbon number increases, the terminal chains become curly and even formed 'U' shape when the terminal chain has more than nine carbon atoms. This observation suggests that increasing the carbon number can promote the structural disorder of terminal alkyl chains and therefore enhance the molecular polarity. Combining the data of dipole moments in Figure 4 and molecular structures in Figure 5, it appears that effect of terminal alkyl chain is biphasic. Elongating the alkyl chains can reduce the molecular dipole moments and improve the flexibility of terminal chain structures. However, when the terminal chains are long enough that can induce disorder, molecular dipole moment will increase as the result of enhanced molecular asymmetry. Therefore, terminal alkyl chain can either enhance or reduce the molecular dipole moment of ABLCs depending on the number of carbon atom, leading to a biphasic effect on the behaviors of nematic phases.

3.3 Effect of changing azo position

Traditionally, ABLCs utilized ester and azo groups as bridging units, in which the azo and ester groups are implemented as side-arms and direct linkages of the central bent core, respectively. ABLC yielded by this approach usually exhibited high melting points and narrow temperature windows of nematic phase, which are unsuitable for practical applications. We postulated that the strong intermolecular forces give raise to these unfavorable characteristics of ABLC and proposed to use two azo bonds as the exclusive linking units with the central bent-core can effectively reduce the intermolecular interactions. Previous studies suggest that changing the position of azo groups

does not improve the mesogenic properties of ABLC.[17,25] However, their investigation focused on the effect of swapping one azo group with ester linkage and did not consider the scenario of linking two azo groups directly to the central bent-core.

To examining our theory, molecular simulations were carried out to compute the dipole moments of central molecular structure of 4-chloro-1,3-diazobenzene and its structural isomer by exchanging the azo linkages with ester bridges. Figure 6 compares the molecular geometry and dipole moments of their *trans* and *cis* isomers. This comparison shows that the dipole moments of central structures with azo linkages are 0.1 ~ 0.4 Debye smaller than that with ester linkages. Small dipole moments indicate weak electrostatic interactions as the main intermolecular interactions in liquid crystal phases, which gives raise to low melting points and wide temperature windows of nematic phase. In addition, when ester groups are directly linked to the central aromatic core, the whole molecule is prone to form an orderly arrangement due to the rotatable ester linkage.

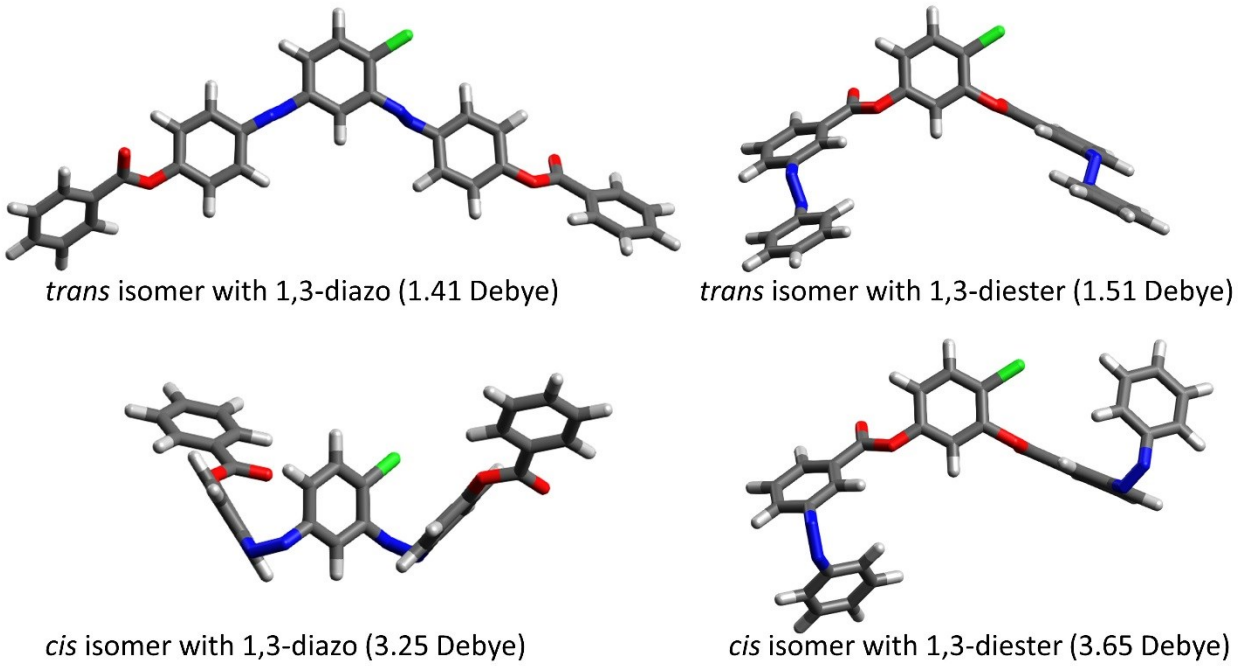

Figure 6. Molecular structures and dipole moments of isomers of central bent-cores in the ground state computed by molecular mechanics simulations.

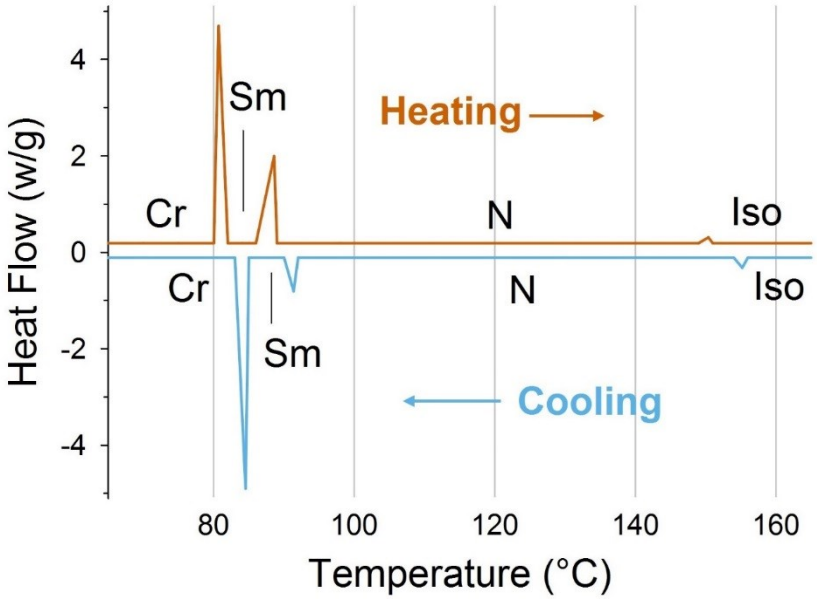

Figure 7. DSC heating and cooling traces of compound **4c**.

Therefore, the temperature windows of mesogenic phases are expected to be narrowed. Therefore, applying azo group as the direct linkage of the central core and ester groups as the side-arm bridges can effectively lower the melting points of ABLCs and broaden the temperature windows of mesogenic phases.

3.4 Additional characterization of compound **4c**

3.4.1 DSC curve and polarized micrograms of **4c**

Because compound **4c** has the lowest melting point and largest temperature windows of mesogenic phases. Additional characterizations were performed on **4c** to represent **4a–4g** compounds. The DSC curves of heating and cooling for compound **4c** is shown in Figure 7. The polarized micrograms of different phases of **4c** on heating are listed in Figure 8. Specifically, **4c** displayed i. a typical columnar texture in smectic phase at 88 °C (Figure 8.1), ii. a schlieren texture in nematic phase at 120 °C (Figure 8.2), and iii. isotropic liquid phase at 155 °C (Figure 8.3).

3.4.2 Photosensitivity of **4c**

Photosensitivity was measured by UV-Vis spectroscopy. As shown in Figure 9, a series of UV-Vis spectra of **4c** (dissolved in ethyl acetate, room temperature) was collected under the UV irradiation (365 nm, 1 mW/cm^2) for 2 s, 5 s, 10 s, and 30 s. All these spectra exhibited a similar pattern: a strong band and a weak band in the regions of 330 – 340 nm and 430 – 450 nm, respectively. The strong band is attributed by the π–π* transition of the azo unit, which indicates the presence of *trans* isomer, while the weak band is ascribed to the *cis* n–π* transition in cis isomer.[8] As the UV irradiation time prolonged, the intensity of the strong band decreased rapidly, whereas the signal of the weak band gradually increased. This pattern indicates the occurrence of *trans* → *cis* photoisomerization.[8] Interestingly, dissolved **4c** reached photostationary state in 10 seconds, significantly faster than reported response rates of similar ABLCs, which are in minutes and even hours.[14,16,17,19–21,25,27,55–58]

Compound **4c** can turn from crystalline solid into nematic phase (Figure 8.4) by heating the pure sample to 95 – 100 °C. Under the UV irradiation (365 nm, 1 nW/cm^2), nematic **4c** became isotropic liquid in 3 seconds. Without the UV irradiation, **4c** restored to nematic phase within 5 seconds under natural light. (Figure 8.5) These phenomena indicate the presence of reversible *trans*

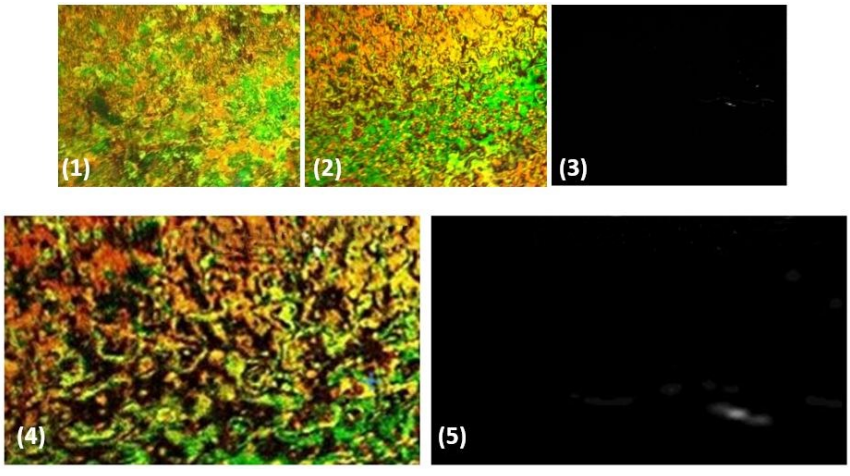

Figure 8. Polarized optical micrograms of compound **4c** under various conditions: (1) smectic textures at 88 °C, (2) nematic textures at 120 °C, (3) isotropic liquid phase at 155 °C, (4) nematic phase at 95 °C, and (5) isotropic liquid phase at 95 °C under UV irradiation.

– *cis* photoisomerization. The UV-induced *cis* isomers can destabilize the orderly arrangement of *trans* isomers in nematic phase and possibly reduced the phase transition temperatures.[4,27] Under visible light, the backward *trans* ← *cis* photoisomerization started and restored the nematic phase of ***4c***.

The ratio of the isomer concentrations can be estimated by the following equation:

$$[cis]_t / [trans]_0 = (1 - A_t / A_0) / (1 - \varepsilon_{cis} / \varepsilon_{trans})^{59,60}$$

where $[cis]_t$ is the concentration of *cis* isomer at time *t*, $[\text{trans}]_0$ the initial concentration of *trans* isomer, A_0 and A_t are the absorbances at the wavelength of the same chromophore of sample compound, in which all sample compounds in solution are either *trans* or *cis* isomers, ε_{cis} and ε_{trans} the molar attenuation coefficients (also known as molar extinction coefficient and molar absorption coefficient) of the *cis* and *trans* isomers at a given wavelength of light, respectively.[60]

Previous studies on similar azobenzene-based compounds report $\varepsilon_{cis} / \varepsilon_{trans}$ ratios of 0.050, 0.053, 0.055, 0.056, and 0.05, corresponding to the UV wavelengths of 320 nm,[60] 325 nm,[60] 355

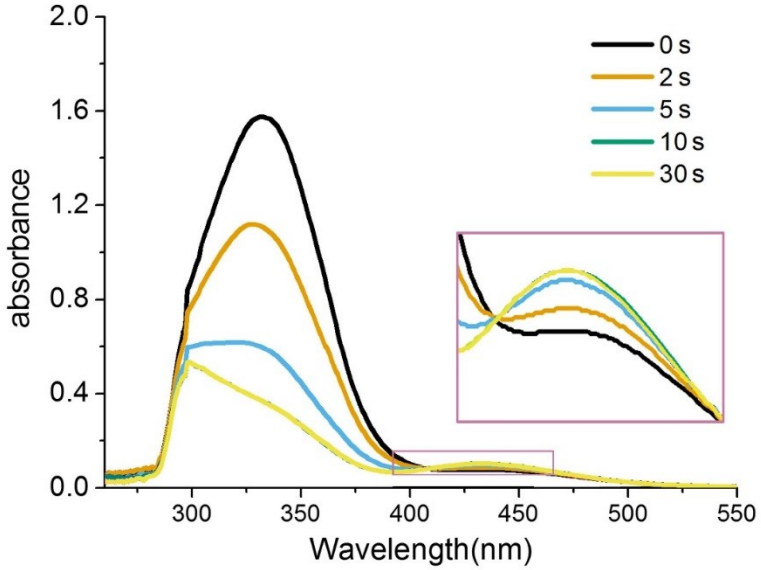

Figure 9. UV-Vis spectra of dissolved compound **4c** under 365 nm UV irradiation for 0 s, 2 s, 5 s, 10 s, and 30 s.

nm,[61] 369.5 nm,[62] and 370 nm,[63] respectively. Therefore, we selected 0.05 as the ε_{cis} / ε_{trans} ratio to estimate the isomer fraction under the irradiation of 365 nm UV. The strong absorption band at 334 nm collected from the 30-second UV irradiation test generated a A_t / A_0 ratio of 0.2348, giving a $[cis]_t$ / $[trans]_0$ ratio of 0.81. This ratio indicates that 81% of nematic **4c** had converted from *trans* to *cis* isomers, which is one of the highest among the reported ratios of similar azobenzene-based compounds.[3,61–66]

4. Conclusion

To date, this is the first study to synthesize ABLCs using two azo bonds as direct linkages of the central bent-core. A series of 4-chloro-1,3-diazobenzene bent-core liquid crystal **4a–4g** were synthesized with different length of terminal alkyl chains. These compounds exhibited broad temperature windows of nematic phases and rapid photoisomerization in seconds. Molecular dipole moments calculated by molecular simulations are strongly correlated with the temperatures of Sm – N phase transition. This finding suggests that electrostatic interactions are the main contributor of intermolecular interactions especially in nematic phases. According to the molecular modeling, the terminal alkyl chains demonstrate a diphasic effect on the molecular dipole due to the structural disorder of overextended alkyl chain, which is consistent with the nematic phase behavior of ABLCs. Moreover, 1,3-diazo at central bent-core can significantly weaken the intermolecular interactions. This research offers valuable implications for advancing future design of azobenzene-based bent-core liquid crystals:

1. Using 1,3-diazobenzene as the bent-core can substantially improve the mesogenic properties and photoisomerization performance.
2. Electrostatic interactions are a controlling factor of mesogenic phase behavior, especially for nematic phase. Molecular polarity can indicate the degree of

intermolecular forces in nematic phase, which can be used as a guideline for future design of ABLC compounds.

3. The synergy between experimental and computational efforts is vital for obtaining mechanistic insights to elucidate mesogenic properties.

Acknowledgments

This work was supported by National Natural Science Foundation of China under Grants 11074054 and 11374067.

Disclosure statement

No potential conflict of interest was reported by the authors.

ORCID

Z. Zhang http://orcid.org/0000-0002-0807-8991

References

(1) *Optical Switching*; El-Bawab, T. S., Ed.; Springer US: Boston, MA, 2006. https://doi.org/10.1007/0-387-29159-8.

(2) De Sio, L.; Ricciardi, L.; Serak, S.; La Deda, M.; Tabiryan, N.; Umeton, C. Photo-Sensitive Liquid Crystals for Optically Controlled Diffraction Gratings. *J. Mater. Chem.* **2012**, *22* (14), 6669. https://doi.org/10.1039/c2jm16077c.

(3) Aronzon, D.; Levy, E. P.; Collings, P. J.; Chanishvili, A.; Chilaya, G.; Petriashvili, G. Trans–Cis Isomerization of an Azoxybenzene Liquid Crystal. *Liquid Crystals* **2007**, *34* (6), 707–718. https://doi.org/10.1080/02678290701267480.

(4) Ikeda, T.; Tsutsumi, O. Optical Switching and Image Storage by Means of Azobenzene Liquid-Crystal Films. *Science* **1995**, *268* (5219), 1873–1875. https://doi.org/10.1126/science.268.5219.1873.

(5) Finkelmann, H.; Nishikawa, E.; Pereira, G. G.; Warner, M. A New Opto-Mechanical Effect in Solids. *Phys. Rev. Lett.* **2001**, *87* (1), 015501. https://doi.org/10.1103/PhysRevLett.87.015501.

(6) Reddy, R. A.; Tschierske, C. Bent-Core Liquid Crystals: Polar Order, Superstructural Chirality and Spontaneous Desymmetrisation in Soft Matter Systems. *J. Mater. Chem.* **2006**, *16* (10), 907–961. https://doi.org/10.1039/B504400F.

(7) Mahimwalla, Z.; Yager, K. G.; Mamiya, J.; Shishido, A.; Priimagi, A.; Barrett, C. J. Azobenzene Photomechanics: Prospects and Potential Applications. *Polym. Bull.* **2012**, *69* (8), 967–1006. https://doi.org/10.1007/s00289-012-0792-0.

(8) Alaasar, M. Azobenzene-Containing Bent-Core Liquid Crystals: An Overview. *Liquid Crystals* **2016**, *43* (13–15), 2208–2243. https://doi.org/10.1080/02678292.2016.1175676.

(9) Merino, E.; Ribagorda, M. Control over Molecular Motion Using the *Cis* – *Trans* Photoisomerization of the Azo Group. *Beilstein J. Org. Chem.* **2012**, *8*, 1071–1090. https://doi.org/10.3762/bjoc.8.119.

(10) Natansohn, A.; Rochon, P. Photoinduced Motions in Azo-Containing Polymers. *Chem. Rev.* **2002**, *102* (11), 4139–4176. https://doi.org/10.1021/cr970155y.

(11) Camacho-Lopez, M.; Finkelmann, H.; Palffy-Muhoray, P.; Shelley, M. Fast Liquid-Crystal Elastomer Swims into the Dark. *Nature Mater* **2004**, *3* (5), 307–310. https://doi.org/10.1038/nmat1118.

(12) Wang, Y.; Li, Q. Light-Driven Chiral Molecular Switches or Motors in Liquid Crystals. *Adv. Mater.* **2012**, *24* (15), 1926–1945. https://doi.org/10.1002/adma.201200241.

(13) Garcia-Amorós, J.; Reig, M.; Castro, M. C. R.; Cuadrado, A.; Raposo, M. M. M.; Velasco, D. Molecular Photo-Oscillators Based on Highly Accelerated Heterocyclic Azo Dyes in Nematic Liquid Crystals. *Chem. Commun.* **2014**, *50* (51), 6704–6706. https://doi.org/10.1039/C4CC01450B.

(14) Sunil, B. N.; Srinatha, M. K.; Shanker, G.; Hegde, G.; Alaasar, M.; Tschierske, C. Effective Tuning of Optical Storage Devices Using Photosensitive Bent-Core Liquid Crystals. *Journal of Molecular Liquids* **2020**, *304*, 112719. https://doi.org/10.1016/j.molliq.2020.112719.

(15) Rahman, M. L.; Asik, J.; Kumar, S.; Tschierske, C. Liquid Crystalline Banana-shaped Monomers Derived from 2,7-naphthalene: Synthesis and Properties. *Liquid Crystals* **2008**, *35* (11), 1263–1270. https://doi.org/10.1080/02678290802513808.

(16) Lutfor, M. R.; Hegde, G.; Kumar, S.; Tschierske, C.; Chigrinov, V. G. Synthesis and Characterization of Bent-Shaped Azobenzene Monomers: Guest–Host Effects in Liquid Crystals with Azo Dyes for Optical Image Storage Devices. *Optical Materials* **2009**, *32* (1), 176–183. https://doi.org/10.1016/j.optmat.2009.07.006.

(17) Nagaveni, N. G.; Raghuvanshi, P.; Roy, A.; Prasad, V. Azo-Functionalised Achiral Bent-Core Liquid Crystalline Materials: Effect of Presence of –N=N– Linkage at Different Locations in the Molecular Architecture. *Liquid Crystals* **2013**, *40* (9), 1238–1254. https://doi.org/10.1080/02678292.2013.805831.

(18) Ghosh, S.; Begum, N.; Turlapati, S.; Roy, S. Kr.; Das, Abhijit. Kr.; Rao, N. V. S. Ferroelectric-like Switching in the Nematic Phase of Four-Ring Bent-Core Liquid Crystals. *J. Mater. Chem. C* **2014**, *2* (3), 425–431. https://doi.org/10.1039/C3TC31800A.

(19) Paterson, D. A.; Xiang, J.; Singh, G.; Walker, R.; Agra-Kooijman, D. M.; Martínez-Felipe, A.; Gao, M.; Storey, J. M. D.; Kumar, S.; Lavrentovich, O. D.; Imrie, C. T. Reversible Isothermal Twist–Bend Nematic–Nematic Phase Transition Driven by the Photoisomerization of an Azobenzene-Based Nonsymmetric Liquid Crystal Dimer. *J. Am. Chem. Soc.* **2016**, *138* (16), 5283–5289. https://doi.org/10.1021/jacs.5b13331.

(20) Alaasar, M.; Poppe, S. Cybotactic Nematic Phases with Wide Ranges in Photoresponsive Polycatenars. *Liquid Crystals* **2019**, 1–11. https://doi.org/10.1080/02678292.2019.1690062.

(21) Alaasar, M.; Prehm, M.; Tschierske, C. Influence of Halogen Substituent on the Mesomorphic Properties of Five-Ring Banana-Shaped Molecules with Azobenzene Wings. *Liquid Crystals* **2013**, *40* (5), 656–668. https://doi.org/10.1080/02678292.2013.767949.

(22) Horčic, M.; Kozmík, V.; Svoboda, J.; Novotná, V.; Pociecha, D. Transformation from a Rod-like to a Hockey-Stick-like and Bent-Shaped Molecule in 3,4′-Disubstituted Azobenzene-Based Mesogens. *J. Mater. Chem. C* **2013**, *1* (45), 7560. https://doi.org/10.1039/c3tc31593b.

(23) Gimeno, N.; Pintre, I.; Martínez-Abadía, M.; Serrano, J. L.; Ros, M. B. Bent-Core Liquid Crystal Phases Promoted by Azo-Containing Molecules: From Monomers to Side-Chain Polymers. *RSC Adv.* **2014**, *4* (38), 19694–19702. https://doi.org/10.1039/C4RA02079K.

(24) Dingemans, T. J.; Murthy, N. S.; Samulski, E. T. Javelin-, Hockey Stick-, and Boomerang-Shaped Liquid Crystals. Structural Variations on *p* -Quinquephenyl †. *J. Phys. Chem. B* **2001**, *105* (37), 8845–8860. https://doi.org/10.1021/jp010869j.

(25) Monika, M.; Prasad, V.; Nagaveni, N. G. Hockey Stick-Shaped Azo Compounds: Effect of Linkage Groups and Their Direction of Linking on Mesomorphic Properties. *Liquid Crystals* **2015**, *42* (10), 1490–1505. https://doi.org/10.1080/02678292.2015.1066889.

(26) Bobrovsky, A.; Shibaev, V.; Hamplová, V.; Bubnov, A.; Novotná, V.; Kašpar, M.; Piryazev, A.; Anokhin, D.; Ivanov, D. Photo-Optical Properties of Amorphous and Crystalline Films of Azobenzene-Containing Photochromes with Bent-Shaped Molecular Structure. *Journal of Photochemistry and Photobiology A: Chemistry* **2016**, *316*, 75–87. https://doi.org/10.1016/j.jphotochem.2015.10.021.

(27) Alaasar, M.; Prehm, M.; Tschierske, C. Helical Nano-Crystallite (HNC) Phases: Chirality Synchronization of Achiral Bent-Core Mesogens in a New Type of Dark Conglomerates. *Chem. Eur. J.* **2016**, *22* (19), 6583–6597. https://doi.org/10.1002/chem.201505016.

(28) Alaasar, M.; Prehm, M.; Brautzsch, M.; Tschierske, C. 4-Methylresorcinol Based Bent-Core Liquid Crystals with Azobenzene Wings – a New Class of Compounds with Dark Conglomerate Phases. *J. Mater. Chem. C* **2014**, *2* (28), 5487–5501. https://doi.org/10.1039/C4TC00533C.

(29) Alaasar, M.; Prehm, M.; May, K.; Eremin, A.; Tschierske, C. 4-Cyanoresorcinol-Based Bent-Core Mesogens with Azobenzene Wings: Emergence of Sterically Stabilized Polar Order in Liquid Crystalline Phases. *Adv. Funct. Mater.* **2014**, *24* (12), 1703–1717. https://doi.org/10.1002/adfm.201302295.

(30) Alaasar, M.; Prehm, M.; Brautzsch, M.; Tschierske, C. Dark Conglomerate Phases of Azobenzene Derived Bent-Core Mesogens – Relationships between the Molecular Structure and Mirror Symmetry Breaking in Soft Matter. *Soft Matter* **2014**, *10* (37), 7285–7296. https://doi.org/10.1039/C4SM01255K.

(31) Yi, W.; Cai, C. Highly Efficient Dinitration of Aromatic Compounds in Fluorous Media Using Ytterbium Perfluorooctanesulfonate and Perfluorooctanesulfonic Acid as Catalysts. *Synthetic Communications* **2006**, *36* (20), 2957–2961. https://doi.org/10.1080/00397910600773700.

(32) Meng, G.; Zheng, M.-L.; Zheng, A.-Q.; Wang, M.; Shi, J. The Novel Usage of Thiourea Nitrate in Aryl Nitration. *Chinese Chemical Letters* **2014**, *25* (1), 87–89. https://doi.org/10.1016/j.cclet.2013.09.003.

(33) Hegde, G.; Rajkumar, Y. A.; Mei, G. S.; Mahmood, S.; Mandal, U. K.; Sudhakar, A. A. Photoisomerization Behavior of Photochromic Amide-Based Azobenzene Dyes Exhibiting H-Bonding Effect: Synthesis and Characterization. *Korean J. Chem. Eng.* **2016**, *33* (4), 1480–1488. https://doi.org/10.1007/s11814-015-0259-8.

(34) Mathews, M.; Kang, S.; Kumar, S.; Li, Q. Designing Bent-Core Nematogens towards Biaxial Nematic Liquid Crystals. *Liquid Crystals* **2011**, *38* (1), 31–40. https://doi.org/10.1080/02678292.2010.524716.

(35) Hanwell, M. D.; Curtis, D. E.; Lonie, D. C.; Vandermeersch, T.; Zurek, E.; Hutchison, G. R. Avogadro: An Advanced Semantic Chemical Editor, Visualization, and Analysis Platform. *J Cheminform* **2012**, *4* (1), 17.

https://doi.org/10.1186/1758-2946-4-17.
(36) *Avogadro: An Open-Source Molecular Builder and Visualization Tool. Version 1.2.0*.
(37) Wang, J.; Wang, W.; Kollman, P. A.; Case, D. A. Automatic Atom Type and Bond Type Perception in Molecular Mechanical Calculations. *Journal of Molecular Graphics and Modelling* **2006**, *25* (2), 247–260. https://doi.org/10.1016/j.jmgm.2005.12.005.
(38) Wang, J.; Wolf, R. M.; Caldwell, J. W.; Kollman, P. A.; Case, D. A. Development and Testing of a General Amber Force Field. *J. Comput. Chem.* **2004**, *25* (9), 1157–1174. https://doi.org/10.1002/jcc.20035.
(39) Boyd, N. J.; Wilson, M. R. Optimization of the GAFF Force Field to Describe Liquid Crystal Molecules: The Path to a Dramatic Improvement in Transition Temperature Predictions. *Phys. Chem. Chem. Phys.* **2015**, *17* (38), 24851–24865. https://doi.org/10.1039/C5CP03702F.
(40) Chami, F.; Wilson, M. R. Molecular Order in a Chromonic Liquid Crystal: A Molecular Simulation Study of the Anionic Azo Dye Sunset Yellow. *J. Am. Chem. Soc.* **2010**, *132* (22), 7794–7802. https://doi.org/10.1021/ja102468g.
(41) Harada, J.; Ogawa, K.; Tomoda, S. Molecular Motion and Conformational Interconversion of Azobenzenes in Crystals as Studied by X-Ray Diffraction. *Acta Crystallogr B Struct Sci* **1997**, *53* (4), 662–672. https://doi.org/10.1107/S0108768197002772.
(42) Biswas, N.; Umapathy, S. Density Functional Calculations of Structures, Vibrational Frequencies, and Normal Modes of *Trans* - and *Cis* -Azobenzene. *J. Phys. Chem. A* **1997**, *101* (30), 5555–5566. https://doi.org/10.1021/jp970312x.
(43) Henderson, P. A.; Seddon, J. M.; Imrie, C. T. Methylene- and Ether-linked Liquid Crystal Dimers II. Effects of Mesogenic Linking Unit and Terminal Chain Length. *Liquid Crystals* **2005**, *32* (11–12), 1499–1513. https://doi.org/10.1080/02678290500284983.
(44) Henderson, P. A.; Niemeyer, O.; Imrie, C. T. Methylene-Linked Liquid Crystal Dimers. *Liquid Crystals* **2001**, *28* (3), 463–472. https://doi.org/10.1080/02678290010007558.
(45) Tschierske, C. Development of Structural Complexity by Liquid-Crystal Self-Assembly. *Angew. Chem. Int. Ed.* **2013**, *52* (34), 8828–8878. https://doi.org/10.1002/anie.201300872.
(46) Neubert, M. E.; Carlino, L. T.; Fishel, D. L.; D'sidocky, R. M. The Effect of Terminal Alkyl Chain Length on Mesomorphic Properties of 4-Alkoxyphenyl-4'-Alkylbenzoates. *Molecular Crystals and Liquid Crystals* **1980**, *59* (3–4), 253–272. https://doi.org/10.1080/00268948008071427.
(47) Inglot, K.; Martyński, T.; Bauman, D. Influence of the Alkyl Chain Length of Some Mesogenic Molecules on Their Langmuir Film Formation Ability. *Liquid Crystals* **2006**, *33* (7), 855–864. https://doi.org/10.1080/02678290600733798.
(48) Stroobants, A.; Lekkerkerker, H. N. W.; Odijk, T. Effect of Electrostatic Interaction on the Liquid Crystal Phase Transition in Solutions of Rodlike Polyelectrolytes. *Macromolecules* **1986**, *19* (8), 2232–2238. https://doi.org/10.1021/ma00162a020.
(49) Meier, G.; Saupe, A. Dielectric Relaxation in Nematic Liquid Crystals. *Molecular Crystals* **1966**, *1* (4), 515–525. https://doi.org/10.1080/15421406608083290.
(50) Vertogen, G.; de Jeu, W. H. *Thermotropic Liquid Crystals, Fundamentals*; Goldanskii, V. I., Schäfer, F. P., Toennies, J. P., Series Eds.; Springer Series in Chemical Physics; Springer Berlin Heidelberg: Berlin, Heidelberg, 1988; Vol. 45. https://doi.org/10.1007/978-3-642-83133-1.
(51) Gelbart, W. M. Molecular Theory of Nematic Liquid Crystals. *J. Phys. Chem.* **1982**, *86* (22), 4298–4307. https://doi.org/10.1021/j100219a007.
(52) Singh, S. Phase Transitions in Liquid Crystals. *Physics Reports* **2000**, *324* (2–4), 107–269. https://doi.org/10.1016/S0370-1573(99)00049-6.
(53) Margenau, H.; Kestner, N. *Theory of Intermolecular Forces*, 2nd ed.; Elsevier, 1969. https://doi.org/10.1016/C2013-0-02436-X.
(54) Stone, A. *The Theory of Intermolecular Forces*, 2nd ed.; Oxford University Press, 2013. https://doi.org/10.1093/acprof:oso/9780199672394.001.0001.
(55) Choi, S.-W.; Izumi, T.; Hoshino, Y.; Takanishi, Y.; Ishikawa, K.; Watanabe, J.; Takezoe, H. Circular-Polarization-Induced Enantiomeric Excess in Liquid Crystals of an Achiral, Bent-Shaped Mesogen. *Angew.*

Chem. Int. Ed. **2006**, *45* (9), 1382–1385. https://doi.org/10.1002/anie.200503767.
(56) Vera, F.; Tejedor, R. M.; Romero, P.; Barberá, J.; Ros, M. B.; Serrano, J. L.; Sierra, T. Light-Driven Supramolecular Chirality in Propeller-Like Hydrogen-Bonded Complexes That Show Columnar Mesomorphism. *Angew. Chem. Int. Ed.* **2007**, *46* (11), 1873–1877. https://doi.org/10.1002/anie.200603796.
(57) Mathews, M.; Zola, R. S.; Yang, D.; Li, Q. Thermally, Photochemically and Electrically Switchable Reflection Colors from Self-Organized Chiral Bent-Core Liquid Crystals. *J. Mater. Chem.* **2011**, *21* (7), 2098–2103. https://doi.org/10.1039/C0JM03479G.
(58) Senyuk, B.; Wonderly, H.; Mathews, M.; Li, Q.; Shiyanovskii, S. V.; Lavrentovich, O. D. Surface Alignment, Anchoring Transitions, Optical Properties, and Topological Defects in the Nematic Phase of Thermotropic Bent-Core Liquid Crystal A131. *Phys. Rev. E* **2010**, *82* (4), 041711. https://doi.org/10.1103/PhysRevE.82.041711.
(59) Fischer, E. Calculation of Photostationary States in Systems A .Dblarw. B When Only A Is Known. *J. Phys. Chem.* **1967**, *71* (11), 3704–3706. https://doi.org/10.1021/j100870a063.
(60) Victor, J. G.; Torkelson, J. M. On Measuring the Distribution of Local Free Volume in Glassy Polymers by Photochromic and Fluorescence Techniques. *Macromolecules* **1987**, *20* (9), 2241–2250. https://doi.org/10.1021/ma00175a032.
(61) Morishima, Y.; Tsuji, M.; Kamachi, M.; Hatada, K. Photochromic Isomerization of Azobenzene Moieties Compartmentalized in Hydrophobic Microdomains in a Microphase Structure of Amphiphilic Polyelectrolytes. *Macromolecules* **1992**, *25* (17), 4406–4410. https://doi.org/10.1021/ma00043a025.
(62) Sasaki, T.; Ikeda, T.; Ichimura, K. Photoisomerization and Thermal Isomerization Behavior of Azobenzene Derivatives in Liquid-Crystalline Polymer Matrixes. *Macromolecules* **1993**, *26* (1), 151–154. https://doi.org/10.1021/ma00053a023.
(63) Wang, W.; Wang, M.-Z. Effect of α-Cyclodextrin on the Photoisomerization of Azobenzene Functionalized Hydroxypropyl Methylcellulose in Aqueous Solution. *Polym. Bull.* **2007**, *59* (4), 537–544. https://doi.org/10.1007/s00289-007-0789-2.
(64) Ya, Q.; Dong, X.-Z.; Chen, W.-Q.; Duan, X.-M. The Synthesis of Aminoazobenzenes and the Effect of Intermolecular Hydrogen Bonding on Their Photoisomerization. *Dyes and Pigments* **2008**, *79* (2), 159–165. https://doi.org/10.1016/j.dyepig.2008.02.004.
(65) Fischer, E. Temperature Dependence of Photoisomerization Equilibria. Part I. Azobenzene and the Azonaphthalenes. *J. Am. Chem. Soc.* **1960**, *82* (13), 3249–3252. https://doi.org/10.1021/ja01498a005.
(66) Naito, T.; Horie, K.; Mita, I. Photochemistry in Polymer Solids. 11. The Effects of the Size of Reaction Groups and the Mode of Photoisomerization on Photochromic Reactions in Polycarbonate Film. *Macromolecules* **1991**, *24* (10), 2907–2911. https://doi.org/10.1021/ma00010a042.